

Supported Catalysts

Fabrication of Nitrogen-Doped Mesoporous-Carbon-Coated Palladium Nanoparticles: An Intriguing Electrocatalyst for Methanol and Formic Acid Oxidation

Chaiti Ray,^[a] Soumen Dutta,^[a] Ramkrishna Sahoo,^[a] Anindita Roy,^[a] Yuichi Negishi,^[b] and Tarasankar Pal^{*[a]}

Abstract: Inspired by the attractive catalytic properties of palladium and the inert nature of carbon supports in catalysis, a concise and simple methodology for in situ nitrogen-doped mesoporous-carbon-supported palladium nanoparticles (Pd/N-C) has been developed by carbonizing a palladium dimethylglyoximate complex. The as-synthesized Pd/N-C has been exfoliated as a fuel cell catalyst by studying the electro-oxidation of methanol and formic acid. The material synthesized at 400 °C, namely, Pd/N-C-400, exhibits superior mass

activity and stability among catalysts synthesized under different carbonization temperatures between 300 and 500 °C. The unique 1D porous structure in Pd/N-C-400 helps better electron transport at the electrode surface, which eventually leads to about five times better catalytic activity and about two times higher stability than that of commercial Pd/C. Thus, our designed sacrificial metal-organic templated direct pathway becomes a promising technique for Pd/N-C synthesis with superior catalytic performances.

Introduction

Supported materials influence the catalytic efficiency of metal nanoparticles by affecting their valence state, size, available surface area, and stability.^[1–3] To capitalize on the advantages of easy recovery and reusability of noble-metal nanocatalysts in heterogeneous catalysis, various organic or inorganic supports, such as zeolites,^[4,5] polymers,^[6] mesoporous silica,^[7] inorganic oxides,^[8] graphene,^[9,10] carbon nanotubes,^[11,12] activated carbon,^[13] and porous carbon,^[14] are now in great demand. Among them, carbon materials have become a popular support candidate for of features including large surface area, tunable functionalities, chemical inertness, easy availability, effective channels, porosity, and cost effectiveness. Furthermore, to harness electron density in the support, heteroatoms such as nitrogen or boron are often utilized as dopants to enhance the catalytic activity in carbon-supported materials. For instance, doping with electron-rich nitrogen atoms results in the increase in π -electron density in carbon supports.^[15,16] This nitrogen doping helps the nanoparticles to adhere strongly onto the carbon support owing to enhanced electrostatic interactions between the support and metal nanoparticles. As a result

of this strong affinity-based interaction, the doped material appears to be a better catalyst.^[17–19] Recently, research into carbon materials as a support for palladium nanocatalysts has been in huge demand and applied in various fields, even in sensing activities,^[20] surface-enhanced Raman scattering spectroscopy (SERS),^[21] hydrogen storage, and batteries,^[22–30] in addition to catalysis^[31–34] and electrocatalysis.^[35–44] Therefore, the selection of nitrogen-doped carbon support for palladium nanoparticles as a catalyst is clear.

The general approach for synthesis of palladium nanoparticles fabricated on carbon supports involves multistep procedures in which separately synthesized carbon materials are mixed with metal nanoparticles.^[26,45] For example, Ramaprabhu et al. synthesized palladium-decorated nitrogen-doped graphene by solar exfoliation of graphene oxide (GO) with a mixture of melamine and PdCl₂.^[30] Wang et al. synthesized Pd@N-doped carbon by means of a two-step procedure: the first step was the preparation of carbon support and the second step was deposition of the palladium nanoparticles on the support.^[46] Wang et al. also prepared Pd@N-doped carbon in a three-step procedure.^[15] First, a mixture of glucose, poly(ionic liquid)s, and borax was treated at 200 °C for 8 h. The obtained product was then carbonized at 550 °C for 4 h and 1000 °C for 1 h to give a nitrogen-doped carbon material. In the third step, palladium was deposited on the support by reducing PdCl₂ with NaBH₄. Feng et al. synthesized porous worm-like palladium nanotubes (Pd WNTs) in a two-step process.^[37] In the first step, the palladium dimethylglyoximate complex was calcined at 450 °C for 2 h in a muffle furnace to give worm-like PdO nanotubes. Then, Pd WNTs were synthesized by the reduction of PdO nanotubes in the presence of NaBH₄.

[a] C. Ray, S. Dutta, R. Sahoo, A. Roy, Prof. Dr. T. Pal
Department of Chemistry, Indian Institute of Technology
Kharagpur (India)
E-mail: tpal@chem.iitkgp.ernet.in

[b] Prof. Dr. Y. Negishi
Department of Applied Chemistry, Tokyo University of Science
Tokyo 1628601 (Japan)

Supporting information for this article can be found under <http://dx.doi.org/10.1002/asia.201600173>.

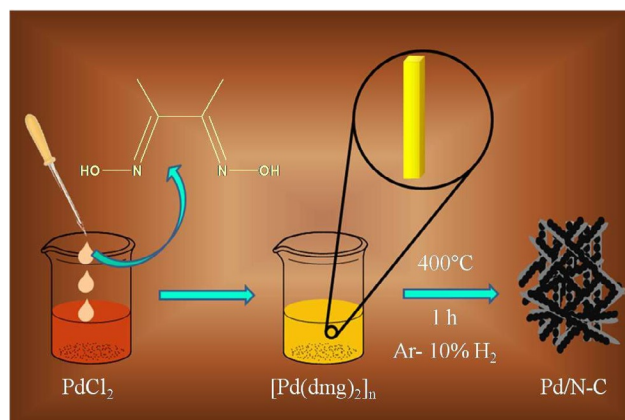
Herein, we report on the development of a novel, inexpensive, cost-effective, easy synthetic strategy for the production of porous nitrogen-doped carbon-supported palladium (Pd/N-C) nanomaterials, involving palladium dimethylglyoximate complex as a precursor, which is easily prepared from dimethylglyoxime (dmg) and PdCl₂ in an acidic solution. The Pd/N-C nanomaterial was obtained after carbonization of palladium dimethylglyoximate complex at 400 °C for 1 h. This method is easy, does not need skilled operation techniques, and is economically viable with an impressive yield of Pd/N-C, even from a waste precipitate from the undergraduate laboratory. No extra precious precursor materials or post-synthetic purification steps are required in this case.

The gradual exhaustion of fossil fuels has resulted in an increase in the demand for renewable energy sources. In recent years, fuel cells have attracted tremendous interest from both energy and environmental considerations by converting chemical energy from fuels such as methanol or formic acid into electrical energy.^[47,48] Platinum is known to be the best catalyst for the alcohol oxidation reaction, but platinum-based catalysts have several disadvantages, such as high cost, low abundance, and easy CO poisoning.^[49] Considering these facts, palladium-based catalysts have benefits in fuel cell applications over platinum-based catalysts in terms of cost and CO poisoning behavior. Nowadays, nitrogen-doped mesoporous-carbon-supported palladium nanostructures are becoming an attractive material in the field of electrocatalysis. Numerous reports are found on alcohol oxidation in basic medium with palladium-based nanomaterial owing to better stability of the electrocatalyst than that in acidic medium.^[35,46,50] Again, for improved stability and robustness in palladium-based catalysts, porous carbon is used as a support for the catalyst.^[30] Herein, the as-prepared nitrogen-doped 1D framework of nanocatalysts with a carbon support are applied as electrocatalysts for fuel cell application. The oxidation of small organic molecules, such as methanol and formic acid, is a notable feature.

Results and Discussion

The dmg precursor is a well-known complexing agent for various metal ions, especially for nickel(II) and palladium(II). In our designed synthetic procedure for porous Pd/N-C nanomaterials, this inexpensive and commonly available compound, dmg, was judiciously introduced as a source of carbon support as well as for nitrogen doping. An aqueous solution of PdCl₂ was used as a precursor for the noble metal. Carbonization of the initially prepared palladium dimethylglyoximate complex from the precursor was performed at 400 °C for 1 h to produce the desired product. The presence of hydrogen in the carbonization environment plays a key role in the reduction of palladium(II) to palladium(0). The effortless and scalable synthetic strategy for producing Pd/N-C is outlined in Scheme 1.

Field-emission (FE) SEM images indicate a smooth surface, with rectangular rod-like structures of palladium dimethylglyoximate complex with diameters of 400–700 nm and lengths of 7–10 μm. The strong interactions between central palladium(II) ions of adjacent square-planar palladium dime-



Scheme 1. Schematic representation of the synthesis of Pd/N-C nanomaterial.

thylglyoximate complexes was supported by observations of Sharpe and Wakefield,^[51] who proved that weak Pd–Pd bonds were present in the palladium dimethylglyoximate complex. This kind of bonding is explained by the facile overlap of filled d_{z²} orbitals of palladium and results in a 1D columnar structure, leading to the formation of [Pd(dmg)₂]_n nanorods. Carbonization of the complex converts the coordination complex into Pd/N-C, with appreciable shrinkage of the primary rod-like structure. Carbonization of the complex at 400 °C for 1 h results in the formation of palladium(0) on the nitrogen-doped carbon support. The FESEM images in Figure 1b and c reveal the porous nature of Pd/N-C at low and medium magnification; this indicates the formation of interconnected chains with retention of the 1D structure. Reduction of palladium(II) and the affinity of palladium for nitrogen engenders the doped structure of Pd/N-C.

Detailed morphology characterization was performed through TEM measurements. Figure 2a–c displays TEM images of the Pd/N-C nanostructure at low, medium, and high resolution, respectively. The porous nature of the Pd/N-C nanostructure is attained through the interconnected chains. The definite contrast discrepancy is accounted in the TEM images, which confirm the porous architecture of the synthesized materials. Figure 2c clearly reveals that the Pd/N-C composite is composed of palladium nanoparticles about 20 nm in diameter uniformly distributed in a continuous carbon support. HRTEM analysis indicates that the sample contains a thin layer of carbon (≈3 nm) coating on the surface of palladium nanoparticles. The carbon matrix is mostly amorphous in nature,

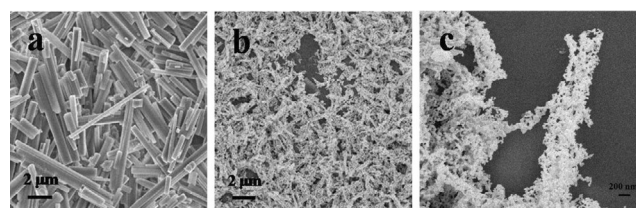


Figure 1. FESEM images of a) [Pd(dmg)₂]_n nanorods and Pd/N-C-400 (Pd/N-C calcined at 400 °C) nanostructure in low (b) and medium (c) resolution.

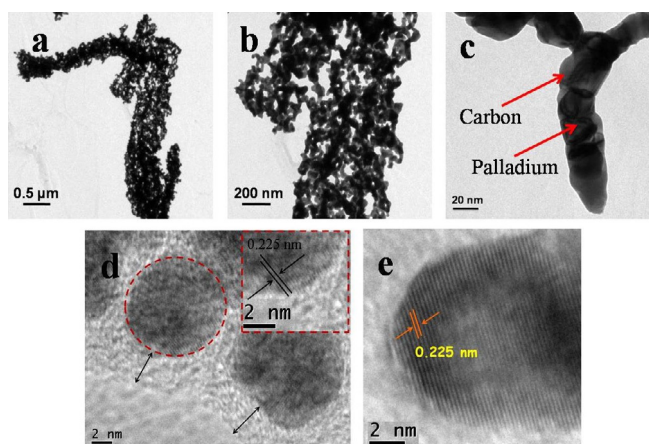


Figure 2. TEM images of the Pd/N-C-400 nanostructure at a) low, b) medium, and c) high magnification. d) High-resolution (HR) TEM image; the fringe spacing of Pd⁰s is given in the inset. e) Close-up view of the fringe spacing of Pd⁰.

whereas palladium nanoparticles are crystalline (Figure 2d). Figure 2e supports the formation of palladium(0) nanoparticles embedded in the carbon material, for which the fringe spacing of 0.225 nm corresponds to the (111) interplanar spacing of palladium nanoparticles. Generally, the type of structure of metal nanoparticles embedded on a carbon support can only be achieved by pyrolysis of metal–organic complexes in an inert atmosphere.^[52] Figure S1 in the Supporting Information presents HRTEM images of Pd/N-C-400 from four different positions. In each image, the red dotted circle represents palladium nanoparticles with diameters of about 17–20 nm and the black arrow indicates the uniform carbon layer of about 3 nm thickness on the palladium nanoparticle surface. Thus, HRTEM analysis proves the formation of a uniform carbon coating on the surface of palladium nanoparticles.

The morphology and composition of the as-synthesized Pd/N-C nanostructures are highly dependent on the carbonization temperature of the palladium dimethylglyoximate complex. To evaluate the effect of temperature on morphology alterations of the interconnected chain, TEM analysis of Pd/N-C-300 and Pd/N-C-500 was carried out and the corresponding TEM images are shown in Figure S2 in the Supporting Information. A question may be asked about the choice of carbonization temperature of the palladium dimethylglyoximate complex. Destruction of the complex skeleton, reduction of palladium(II) to palladium(0) and retention of the porous carbon skeleton are the desired features of the prescribed thermal treatment. An investigation of the retention of parental morphology, that is, a 1D structure with porous architecture, is of prime importance in the present case. To arrive at the desired morphology, we conducted thermolysis of the complex at different temperatures. As expected, the lower temperature (300 °C) could not carbonize the rod-like morphology of the palladium dimethylglyoximate complex quantitatively (Figure S2a in the Supporting Information). However, the higher temperature (≈ 500 °C) destroys the 1D network of Pd/N-C (Figure S2b in the Supporting Information). Thus, retention of 1D network with meso-

porous interconnections for effective electron transport and an admirable catalytic activity of Pd/N-C are achieved if the complex is carbonized at 400 °C.

To demonstrate the nature of doping in the as-synthesized carbonaceous materials, elemental area mapping analysis of carbon, nitrogen, and palladium was performed by means of scanning transmission electron microscopy (STEM). Figure 3 displays a homogeneous distribution of all elements over a 1D matrix. The linescan and energy-dispersive X-ray spectroscopy (EDXS) analyses support the synthesis of Pd/N-C quantitatively (Figure S3 in the Supporting Information).

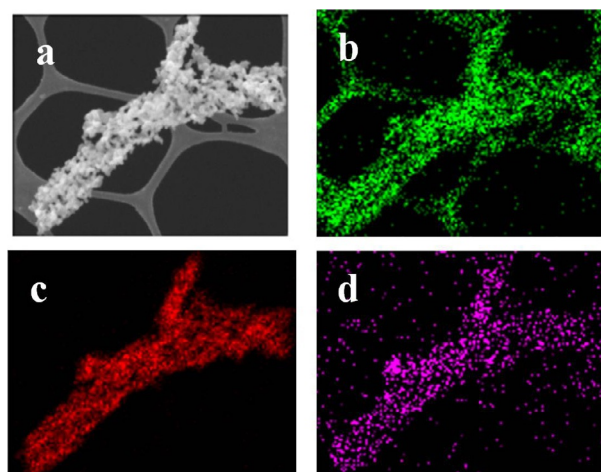


Figure 3. a) STEM image of the Pd/N-C-400 nanostructure and the corresponding mapping images of the elements b) carbon, c) palladium, and d) nitrogen.

To determine the palladium content (in wt%) in the Pd/N-C nanocomposites in the bulk phase, inductively coupled plasma mass spectrometry (ICP-MS) analysis was performed. The results show that the palladium contents in Pd/N-C-300, -400, and -500 are 41.87, 35.55, and 34.82 wt%, respectively. The palladium content (wt%) in Pd/N-C determined by ICP-MS is similar to that determined by EDXS analysis.

BET analysis was performed to investigate the porous nature and specific surface area of the Pd/N-C-400 nanostructure. The nitrogen gas adsorption–desorption isotherm of this porous material is shown in Figure 4a, from which the IV-type isotherm confirms the mesoporous nature of the material with a clear H₁-type hysteresis loop in the 0.5–1.0 P/P_0 range.^[53] This material shows a nitrogen gas uptake capacity of about 136 cc g⁻¹ and a calculated specific surface area of 124.095 m² g⁻¹ with a pore volume 0.158 cc g⁻¹. According to the Barret–Joyner–Halenda (BJH) plot, the calculated half-pore diameter of the material is 1.802 nm. The pore size distribution graph in Figure 4b confirms the mesoporous nature of the material. Figure S4a and c in the Supporting Information shows the nitrogen adsorption–desorption isotherms of the Pd/N-C-300 and -500 nanostructures with surface areas of 33.38 and 60.19 m² g⁻¹, respectively. The calculated half-pore widths are 1.97 and 1.95 nm for the Pd/N-C-300 and -500 nanostructures, respectively (Figure S4b and d in the Supporting Information).

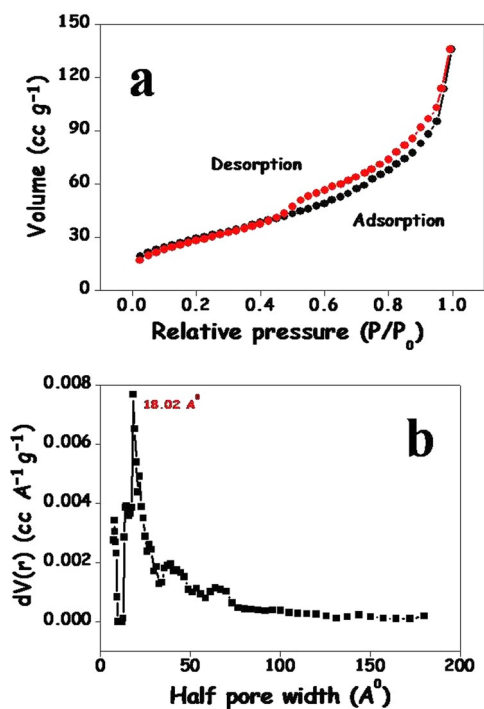


Figure 4. a) Nitrogen adsorption-desorption isotherm and b) pore size distribution plot of the porous Pd/N-C-400 nanostructure.

Thus, Pd/N-C-400 has a higher specific surface area than those of the other two as-prepared nanostructures.

The XRD pattern in Figure 5 confirms the crystalline nature of the as-prepared Pd/N-C samples; sharp diffraction peaks at 40.1 (111), 46.5 (200), 68.2 (220), 82.3 (311), and 86.6° (222) are in good agreement with characteristic peaks of palladium (JCPDS, card no. 05-0681) and a broad peak at 23.4° (002) indicates the presence of graphitic carbon. For comparison, the XRD pattern of [Pd(dmg)₂]_n is also provided, in which the strong peak at about 10° confirms the formation of a metal-organic complex; this peak was found to disappear after carbonization, which confirmed the complete conversion of metal-organic complex into our desired Pd/C material. The palladium nanoparticle size in the Pd/N-C-400 nanostructure can be evaluated by using the Scherrer equation [Eq. (1)]:^[54,55]

$$L = \frac{0.9 \lambda_{K\alpha 1}}{B_{2\theta} \cos \theta_{\max}} \quad (1)$$

in which L is the size of palladium nanoparticles, $\lambda_{K\alpha 1}$ is the X-ray wavelength ($\lambda = 0.154$ nm), $B_{2\theta}$ is the half-peak width, and θ_{\max} is the Bragg angle. The calculated palladium nanoparticle size is 19.2 nm for the Pd/N-C-400 nanostructure, which is in good agreement with TEM results.

X-ray photoelectron spectroscopy (XPS) analysis was executed to scrutinize the electronic state and bonding configurations of the elements (Pd, N, C) present in the as-synthesized materials (Figure 6). The binding energy peaks of C 1s in the XPS spectrum were observed at 284.6, 285.8, and 288.8 eV; these could be attributed to the formation of the sp²-graphitic structure, C–N/C–O/C–C, and C=N/C=O, respectively. The in situ sp²-graphitic structure formation facilitates electron transfer throughout the nanostructure by improving the electron conductivity properties. Analysis of the Pd 3d XPS spectra confirms the formation of pure palladium(0) in the Pd/N-C materi-

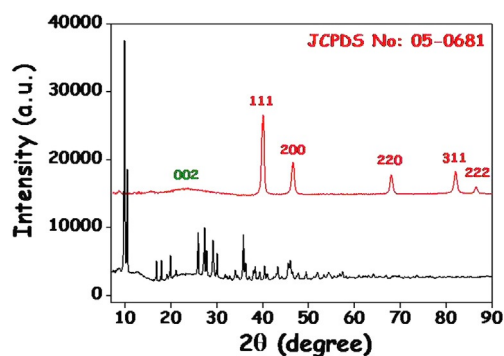


Figure 5. XRD pattern of [Pd(dmg)₂]_n (black) and Pd/N-C-400 (red).

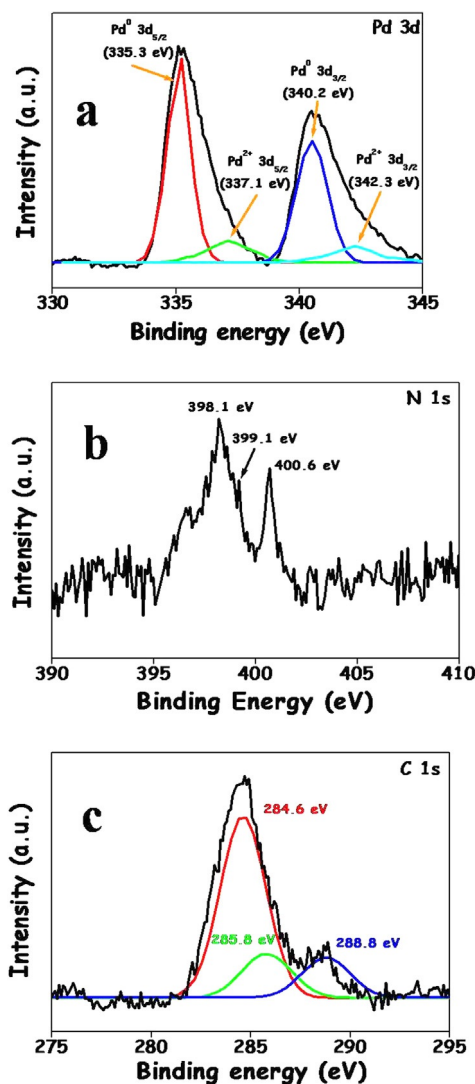


Figure 6. XPS spectra of a) Pd 3d, b) N 1s, and c) C 1s elements of Pd/N-C-400.

als with increasing annealing temperature. The binding energies of Pd⁰ 3d_{5/2} and Pd⁰ 3d_{3/2} for Pd/N-C-400 and -500 are observed to be comparable (335.3 and 340.4 eV for Pd/N-C-400; 335.4 and 340.6 eV for Pd/N-C-500), whereas there is a positive shift in the case of Pd/N-C-300 (336.6 and 341.7 eV). Again, the prominent peaks for the Pd 3d_{5/2} and Pd 3d_{3/2} electronic states of palladium(II) appear at around 338.7 and 341.7 eV in the case of Pd/N-C-300. Deconvolution of the Pd 3d XPS spectrum shows almost the same content of Pd⁰ (52.7%) and Pd²⁺ (47.3%) in the Pd/N-C-300 material. XPS measurements of Pd/N-C-400 show that most of the palladium species are present as palladium(0) nanoparticles (85.1%), with a small amount of Pd²⁺ (14.9%) in the nitrogen-doped carbon support. Upon increasing the carbonization temperature to 500 °C, characteristic palladium peaks indicates a majority of palladium(0) (89%) species in the Pd/N-C-500 material. The binding energies of N 1s for pyridinic, pyrrolic, and quaternary-N groups experience a positive shift with increasing annealing temperature owing to electron density transfer from nitrogen to palladium. Lowering of the binding energy of Pd 3d in Pd/N-C-400 and -500 is in good agreement with previous reports by the groups of Wang^[46] and Zhou.^[56] The pyridinic and pyrrolic nitrogen atoms can donate their π-electron density to support the carbon network. As a result, the nitrogen-doped carbon support stabilizes palladium(0) by preventing its reoxidation and facilitates the reduction of palladium(II) to palladium(0).^[57,58]

The XPS spectra of Pd 3d, C 1s, and N 1s of various as-synthesized materials are shown in Figure S5 in the Supporting Information. The contents of palladium, nitrogen, and carbon in as-synthesized Pd/N-C-300, -400, and -500 are summarized in Table S1 in the Supporting Information. These results are in good agreement with those obtained by ICP-MS analysis. As a result, temperature-dependent, as-synthesized Pd/N-C nanostructures vary in catalytic activity, as discussed below.

Electrocatalysis

The electrocatalytic activity of as-prepared Pd/N-C was tested by considering the methanol oxidation reaction (MOR) and formic acid oxidation reaction (FAOR) as model reactions for fuel cell applications. These small organic molecules were electrochemically oxidized to convert their chemical energy into clean electrical energy, and the whole process was studied by cyclic voltammetry (CV). The influence of annealing temperature on the catalytic behavior of our catalysts was also investigated. Commercial 20 wt% Pd/C (Pd/C) was used as a reference catalyst to estimate the effectiveness of our synthesized material.

The electrocatalytic efficiency of a catalyst is highly dependent on the available electrochemically active surface area (ECSA). The ECSAs of as-prepared nanocatalysts and Pd/C were evaluated from cyclic voltammograms by using a modified glassy carbon electrode (GCE) in 1 M KOH at a scan rate 50 mV s⁻¹ (Figure 7). The ECSA values were calculated by using Equation (2):

$$\text{ECSA} = Q_0/q_0 \quad (2)$$

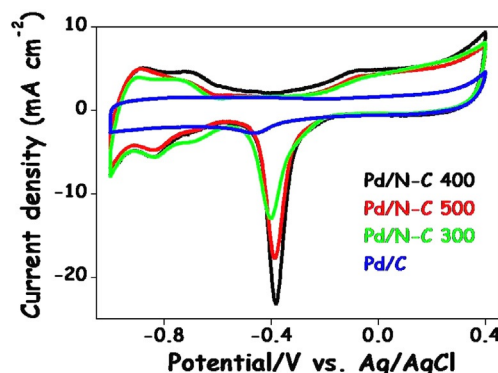


Figure 7. Cyclic voltammograms of GCEs modified with four catalysts in 1 M KOH at a scan rate 50 mV s⁻¹. The current density was calculated by considering the surface area of GCE (0.07 cm²).

in which Q_0 is the surface charge obtained from the area under the CV curves of palladium oxide reduction and q_0 represents the charge required for desorption of a monolayer of oxygen from a clean palladium surface, that is, 424 $\mu\text{C cm}^{-2}$.^[35] In all cases, 7 μg catalyst was used. For ECSA calculations, ICP-MS analysis data for the palladium content (wt%) in Pd/N-C was used. Cyclic voltammograms of all catalysts in KOH medium are shown in Figure 7. The CV profile of commercial Pd/C in KOH medium demonstrates a clear peak for PdO reduction at -0.46 V versus Ag/AgCl (Figure S6 in the Supporting Information). The hydrogen desorption region is not prominent, but a small hump is found. For as-synthesized Pd/N-C catalysts, peaks of both PdO reduction and the hydrogen region are prominent.

This type of anomaly in the cyclic voltammograms is mainly found owing to differences in electrocatalytic activities. During the cathodic sweep, the peak for palladium oxide reduction appeared at around -0.39 V versus Ag/AgCl for Pd/N-C-400; this is nearly the same as that for Pd/N-C-300 and identical to that for Pd/N-C-500. Moreover, Pd/N-C-400 has a palladium oxide reduction peak at a potential about 70 mV higher than that of commercial Pd/C (-0.46 V), which indicates less interaction between metal and oxygen in the case of the as-synthesized Pd/N-C-400 nanostructure. The ECSA values of Pd/N-C-400 (160.71 m² g⁻¹) are 1.9 and 1.5 times higher than those of Pd/N-C-300 (84.95 m² g⁻¹) and -500 (103.91 m² g⁻¹), respectively. It is important to note that all Pd/N-C catalysts have higher ECSA values than that of Pd/C (59.4 m² g⁻¹). This information leads us to draw the conclusion that Pd/N-C-400 has more electrocatalytically active sites than other samples as a result of its highly porous structure from the self-assembly of the unique chain-like morphology.^[59]

In Figure 8a, the oxidation of methanol by Pd/N-C shows two oxidation peaks. The peak of the forward scan arises because of methanol oxidation to form CO₂ and the peak for the reverse scan indicates the oxidation of carbonaceous species generated during methanol oxidation in the forward scan.

CV measurements at a scan rate of 50 mV s⁻¹ exhibit specific peak current densities for Pd/N-C-400 that are 2, 3, and 8 times higher than those of Pd/N-C-500, -300, and commercial Pd/C,

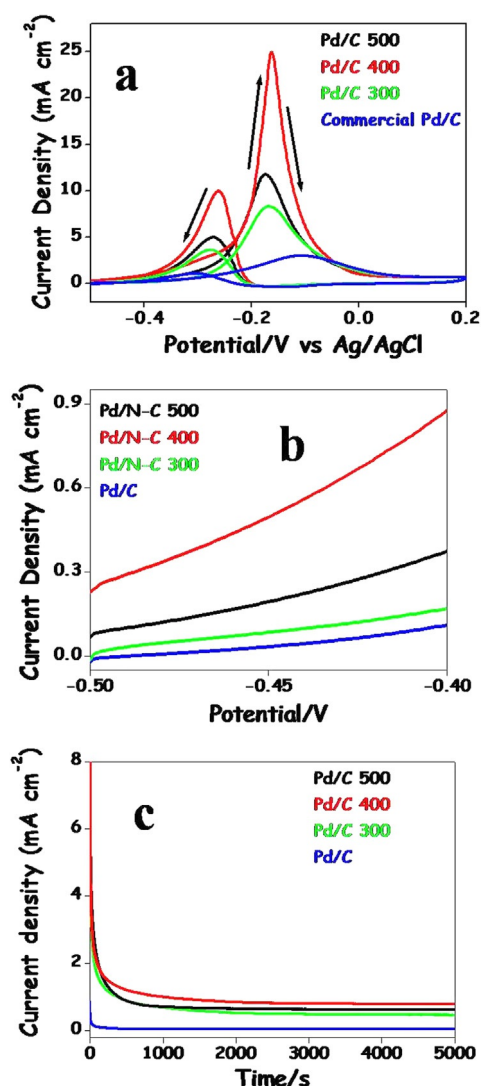


Figure 8. a) Cyclic voltammograms of various catalysts with a mixture of 0.5 M KOH and 0.5 M methanol at a scan rate 50 mV s⁻¹. b) Onset potentials of four electrocatalysts for methanol oxidation in alkaline medium. c) Chronoamperometric (CA) curves with various catalysts during the MOR at an applied potential of -0.20 V. In each case, current density is plotted with respect to the surface area of the GCE (0.07 cm²).

respectively. In addition, as seen in Figure 8b, the onset potential of methanol oxidation in alkaline medium for Pd/N-C-400 is significantly lower than those of Pd/N-C-500, -300, and commercial Pd/C; this supports the higher catalytic efficiency of Pd/N-C-400 for methanol oxidation over other catalysts. The oxidation peak potential in the forward scan for Pd/N-C-400 is observed at -0.17 V, which is similar to those of other catalysts synthesized under different annealing temperatures, except for

commercial Pd/C (-0.1 V). Again, to determine the actual electrocatalytically active site in the composite, the MOR has been performed by using nitrogen-doped carbon material as a catalyst. As shown in Figure S7 in the Supporting Information, nitrogen-doped carbon material has a negligible specific peak current density compared with that of Pd/N-C-400. Thus, from the above results, we can infer that palladium atoms act as the catalytically active site in the Pd/N-C nanostructure. The mass activities (normalized with respect to the amount of catalyst) at -0.164 V (vs. Ag/AgCl) of the four catalysts are 760.8, 358.5, 259.1, and 158.3 mA mg_{Pd}⁻¹ for Pd/N-C-400, -500, -300, and commercial Pd/C, respectively; these values suggest better mass utilization of the precious palladium element to gain maximum efficiency. Additionally, to investigate the tolerance level of all catalysts, including commercial Pd/C, towards accumulated CO during catalysis, the ratio of forward and backward currents (*I_f/I_b*) was calculated. A higher *I_f/I_b* ratio implies greater antipoisoning activity of the catalyst. Herein, as-synthesized Pd/N-C-400 exhibits a higher *I_f/I_b* ratio (2.52; Table 1) than those of the other catalysts, that is, Pd/N-C-300 (2.26), Pd/N-C-500 (2.32), and commercial Pd/C (2.18). Moreover, Pd/N-C-400 demonstrates a higher specific activity (normalized with respect to ECSA) than those of the other three catalysts (Table 1).

The chain-like array of Pd/N-C-400 increases the electro-oxidation behavior towards CH₃OH by lowering the onset potential and exhibiting significantly higher peak current density than the other three tested catalysts. The electrocatalytic activity of Pd/N-C-400, in terms of mass activity, is higher than those of various reports in the literature reports,^[35,41,60-66] as shown in Table 2, which suggests that our synthesized material shows better catalytic activity for methanol oxidation.

Herein, the electrocatalytic activity of Pd/N-C and Pd WNTs (synthesized according to the procedure of Feng et al.^[37]) were investigated towards methanol oxidation in alkaline medium (Figure S8 in the Supporting Information). The Pd/N-C catalyst shows a higher mass activity (760.8 mA mg_{Pd}⁻¹) than that of Pd WNTs (149.6 mA mg_{Pd}⁻¹). Thus, the above-stated synthetic procedure to prepare Pd/N-C has delivered a new and excellent electrocatalyst with enhanced mass activity.

Furthermore, the electrochemical stability of the catalysts for methanol oxidation was studied by means of the CA method at a given potential -0.2 V in 0.5 M KOH and 0.5 M CH₃OH. The results in Figure 8c reveal an initial rapid decrease in current density for all catalysts, owing to the chemisorption of carbonaceous materials on the surface of the palladium catalyst during electro-oxidation, and then a slower current density decay of Pd/N-C-400 with time (5000 s) in comparison with Pd/N-C-500, -300, and Pd/C. This data supports the higher restraint of Pd/N-C-400 towards as-produced carbonaceous species,

Table 1. A comparison of the electrocatalytic activity of four catalysts towards the MOR.

Catalyst	ECSA _{Pd} [m ² g ⁻¹]	Current density [mA cm ⁻²]	<i>I_f/I_b</i>	Mass activity [mA mg _{Pd} ⁻¹]	Specific activity [mA cm ⁻²]
Pd/N-C-300	84.95	8.29	2.26	259.1	0.305
Pd/N-C-400	160.71	24.92	2.53	760.8	0.473
Pd/N-C-500	103.91	11.78	2.32	358.5	0.345
Pd/C	59.4	3.01	2.18	158.3	0.266

Material ^[a]	Mass activity [mA mg _{Pd} ⁻¹]	Ref.
Pd-chestnutbur	566.3	[35]
HPN-CNT	≈ 300	[41]
PdNP/low-defect graphene	128.8	[60]
Pd/XC-72	280	[61]
Pd/CMS	500	[62]
Pt–Pd NPs/RGO	198	[63]
Pd–Ni–P NPs/C	≈ 380	[64]
Pd NPs on ordered mesoporous carbon	197	[65]
Pd ₃₄ Pt ₆₆ NPs	≈ 100	[66]
Pd/N-C-400	760.8	this work

[a] HPN-CNT = hollow palladium nanosphere–carbon nanotube, Pd/CMS = palladium carbon microspheres, RGO = reduced graphene oxide.

such as CO, during methanol oxidation in alkaline medium compared with other catalysts. The stability of the electrocatalysts was investigated by comparing the CV profiles of methanol electro-oxidation before and after 1500 cycles. Figure S9 in the Supporting Information reveals that the decay of the original current density of Pd/N-C-400 is about 45.5%, whereas Pd/N-C-500, -300, and commercial Pd/C exhibit decreases in current density of about 68.4, 85.5, and 89.3%, respectively. The methanol electro-oxidation reaction was also performed in alkaline medium with commercial Pt/C as catalyst. The CV measurement clearly reveals a specific peak current density 2.1 times lower (11.9 mA cm⁻²) and a mass activity 1.3 times lower (600 mA mg_{Pt}⁻¹) for commercial Pt/C than those for Pd/N-C-400. In Figure 7e, the CV profile of the MOR represents about 87% decay in current density after 1500 cycles. Thus, the above results support the excellent electrocatalytic activity and stability of as-synthesized Pd/N-C-400 towards the MOR.

The annealing temperature tunes the catalytic activities of the synthesized Pd/N-C nanostructures. Heating the palladium dimethylglyoximate complex at 300 °C fails to convert it completely into the corresponding Pd/C-N-300 sample, as confirmed by TEM and XPS analyses, whereas the synthesized material lost the unique arrangement upon heating at 500 °C. On the other hand, Pd/N-C-400 possesses a majority of palladium(0) content with an exclusive 1D porous architecture and electro-active sites that result in superior electrocatalytic activities and outstanding durability. TEM images of Pd/N-C-400 after the 1st and 1500th cycles of MOR (Figure S10 in the Supporting Information) demonstrate insignificant changes in the morphology to ensure the robustness of the as-synthesized catalyst.

Herein, the electro-oxidation properties of carbon-supported palladium catalysts was again investigated with formic acid in alkaline medium. The low toxicity, non inflammability, and low penetration efficiency makes formic acid a perfect candidate as a fuel in polymer electrolyte membrane fuel cells.^[38,67] The low cost and lower CO poisoning of palladium compared with platinum supports the use of as-synthesized Pd–N/C as a catalyst for the FAOR.

The cyclic voltammogram of 0.25 M formic acid in the presence of 0.5 M KOH at a scan rate 50 mVs⁻¹ (Figure 9a) shows a peak for formic acid oxidation at –0.345 V in the forward scan. On the backward scan, the peak near –0.374 V arises owing to the further oxidation of carbonaceous intermediates to form CO₂.

The Pd/N-C-400 catalyst exhibits an onset potential at –0.84 V, which is 0.19 V lower than that of Pd/C. Furthermore, the formic acid oxidation peak of Pd/N-C-400 has a susceptibility to be more negative than with the other three catalysts, which supports the proposal of the best electrocatalytic oxidation activity of Pd/N-C-400 towards formic acid.

The mass activity of Pd/N-C-400 (525.7 mA mgPd⁻¹) is 1.6, 2.4, and 5 times higher than those of Pd/N-C-500, -300, and Pd/C, respectively (Table 3). Also, the specific activity of Pd/N-C-400 (0.327 mA cm⁻²) is 0.97, 1.3, and 1.85 times higher than those of Pd/N-C-500, -300, and Pd/C, respectively (Table 3). Figure S11 in the Supporting Information shows a comparison of the CV profiles of as-synthesized Pd/N-C-300, -400, -500, and commercial Pd/C catalysts with respect to mass activity and specific activity for the electro-oxidation of methanol and formic acid.

The CA data reveals that the current density decreases sharply with time and reaches a plateau after about 500 s for all Pd/N-C and Pd/C catalysts (Figure 9b). A magnified view reveals the comparatively higher stability of Pd/N-C-400 than the other tested materials (Figure 9b, inset). These results provide direct evidence of the better electrocatalytic performance and

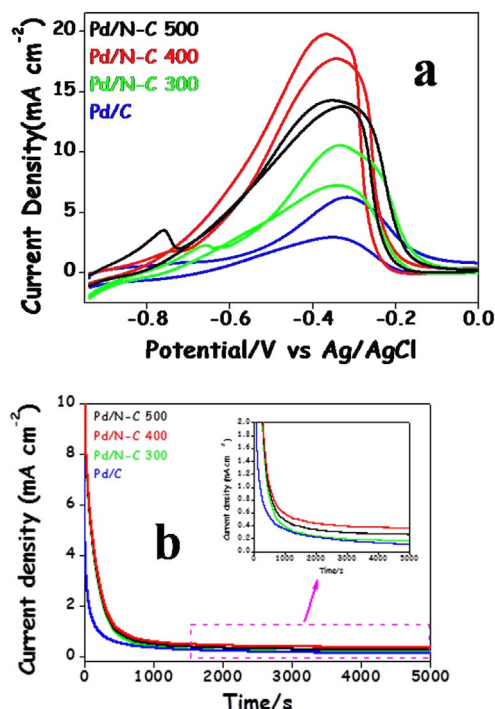


Figure 9. a) Cyclic voltammograms of four catalysts in 0.25 M formic acid and 0.5 M KOH at 50 mVs⁻¹. b) CA curves with various catalysts during the FAOR at an applied potential of –0.35 V (inset shows an enlarged view of *i* versus time curve). In each case, the current density is plotted with respect to the surface area of the GCE (0.07 cm²).

Table 3. A comparison of the mass activity and specific activity values of four catalysts towards the FAOR.

Catalyst	ECSA _{Pd} [m ² g ⁻¹]	Mass activity [mA mg _{Pd} ⁻¹]	Specific activity [mA cm ⁻²]
Pd/N-C-300	84.95	219.1	0.257
Pd/N-C-400	160.71	525.7	0.327
Pd/N-C-500	103.91	328.6	0.316
Pd/C	59.4	105.2	0.177

stability of the product obtained at an annealing temperature of 400 °C, namely, Pd/N-C-400, than those obtained at other temperatures (Pd/N-C-500, Pd/N-C-300).

The better electrocatalytic activity of the as-synthesized Pd/N-C-400 catalyst than that of commercial Pd/C can be explained by considering electronic aspects. When electron-rich nitrogen atoms are introduced into palladium nanoparticles embedded in a carbon matrix, a shift in the d band of palladium takes place and, as a result, the Pd⁰3d_{5/2} peak (335.3 eV) of Pd/N-C-400 is negatively shifted by about 0.5 eV relative to that of commercial Pd/C (335.8 eV; Figure S12 in the Supporting Information). Therefore, nitrogen doping provides a bigger electron-donation effect towards palladium nanoparticles, leading to improved electrocatalytic activity of Pd/N-C-400.

Conclusion

We reported a facile and simple reaction strategy for the formation of in situ Pd/N-C through carbonizing the metal-organic complex [Pd(dmg)₂]_n at 400 °C. The as-synthesized Pd/N-C samples acted as excellent electrocatalysts with superior stability towards methanol and formic acid oxidation in alkaline medium than that of Pd/C, owing to higher electrochemical active surfaces as a result of the 1D nanostructure. This superb electrocatalytic activity makes the porous Pd/N-C nanostructure a promising electrocatalyst for the construction of an efficient fuel cell. The porous Pd/N-C nanostructure can also be used as a useful catalyst in Suzuki coupling reactions under ambient conditions.

Experimental Section

Materials and Instruments

Information regarding materials and instruments are briefly discussed in the Supporting Information.

Synthesis of Pd/N-C

An aliquot (20 mL) of a 10⁻² M solution of dmg was prepared in ethanol. The solution was added dropwise to a 10⁻² M solution of PdCl₂ (10 mL; in water) and immediately a golden yellow precipitate formed. The precipitate was collected by filtration and washed several times with distilled water and dried at 80 °C. Carbonization of the sample was performed in a tube furnace under a mixture of Ar/H₂ (Ar/H₂ = 90:10 vol%) at different temperatures (300, 400, and 500 °C) for 1 h. The obtained materials were labeled Pd/N-C-300,

Pd/N-C-400, and Pd/N-C-500, respectively, according to the carbonization temperature.

Electrochemical Measurements

The electrochemical behavior of Pd/N-C was investigated by using a three-electrode cell in a CHI 660E system with a GCE as a working electrode, a platinum counter electrode, and a saturated solution of Ag/AgCl (saturated KCl) as a reference electrode. First, the GCE electrode was cleaned by polishing with 1, 0.3, and 0.05 μm alumina powder consecutively. Then, under ultrasonic conditions, the electrode was cleaned with distilled water and absolute ethanol, respectively, for 10 min and completely dried in air at room temperature. For electro-oxidation experiments, Pd/N-C catalysts dispersed in water (7 μL, 1 mg mL⁻¹) were drop-cast on the GCE and dried in air for 3 h. In this case, as a binder of the catalyst on the GCE, a 0.01% aqueous solution of Nafion (7 μL) was applied. Then, the completely dried GCE was introduced into the three-electrode setup and, with a fixed scan rate of 50 mV s⁻¹, all CV studies were performed in different electrolyte solutions.

Acknowledgements

We are thankful to the DST and CSIR, New Delhi, India, for financial assistance, and the IIT Kharagpur for instrumental support. We also acknowledge Prof. S. B. Majumder (IIT Kharagpur) for his help in annealing the palladium dimethylglyoximate complex, and Prof. G. Mohan Rao (IISC, Bangalore) for the XPS analyses of the Pd/N-C nanostructures.

Keywords: electrochemistry · doping · nanoparticles · palladium · supported catalysts

- [1] S. Song, S. Yin, Z. Li, P. K. Shen, R. Fu, D. Wu, *J. Power Sources* **2010**, *195*, 1946–1949.
- [2] J. Yang, C. Tian, L. Wang, H. Fu, *J. Mater. Chem.* **2011**, *21*, 3384–3390.
- [3] X. S. Zhao, W. Z. Li, L. H. Jiang, W. J. Zhou, Q. Xin, B. L. Yi, G. Q. Sun, *Carbon* **2004**, *42*, 3263–3265.
- [4] L. Djakovitch, K. Koehler, *J. Am. Chem. Soc.* **2001**, *123*, 5990–5999.
- [5] X. Liu, W. Liu, J. Li, Y. Zhang, L. Lang, L. Ma, B. Zhang, *Ind. Eng. Chem. Res.* **2010**, *49*, 8826–8831.
- [6] Y. Yang, S. Ogasawara, G. Li, S. Kato, *J. Mater. Chem. A* **2013**, *1*, 3700–3705.
- [7] S. El Hankari, A. E. Kadib, A. Finiels, A. Bouhaouss, J. J. E. Moreau, C. M. Crudden, D. Brunel, P. Hesemann, *Chem. Eur. J.* **2011**, *17*, 8984–8994.
- [8] P. D. Stevens, J. Fan, H. M. R. Gardimalla, M. Yen, Y. Gao, *Org. Lett.* **2005**, *7*, 2085–2088.
- [9] G. M. Scheuermann, L. Rumi, P. Steurer, W. Bannwarth, R. Mülhaupt, *J. Am. Chem. Soc.* **2009**, *131*, 8262–8270.
- [10] S. Moussa, A. R. Siamaki, B. F. Gupton, M. S. El-Shall, *ACS Catal.* **2012**, *2*, 145–154.
- [11] A. R. Siamaki, Y. Lin, K. Woodberry, J. W. Connell, B. F. Gupton, *J. Mater. Chem. A* **2013**, *1*, 12909–12918.
- [12] B. Cornelio, G. A. Rance, M. Laronze-Cochard, A. Fontana, J. Sapi, A. N. Khlobystov, *J. Mater. Chem. A* **2013**, *1*, 8737–8744.
- [13] X. Sun, Y. Li, *Angew. Chem. Int. Ed.* **2004**, *43*, 597–601; *Angew. Chem.* **2004**, *116*, 607–611.
- [14] P. Veerakumar, R. Madhu, S.-M. Chen, V. Veeramani, C.-T. Hung, P.-H. Tang, C.-B. Wang, S.-B. Liu, *J. Mater. Chem. A* **2014**, *2*, 16015–16022.
- [15] P. Zhang, Y. Gong, H. Li, Z. Chen, Y. Wang, *Nat. Commun.* **2013**, *4*, 1593.
- [16] P. Chen, L. M. Chew, A. Kostka, M. Muhler, W. Xia, *Catal. Sci. Technol.* **2013**, *3*, 1964–1971.
- [17] R. R. Salunkhe, J. Tang, Y. Kamachi, T. Nakato, J. H. Kim, Y. Yamauchi, *ACS Nano* **2015**, *9*, 6288–6296.

- [18] J. Tang, R. R. Salunkhe, J. Liu, N. L. Torad, M. Imura, S. Furukawa, Y. Yamauchi, *J. Am. Chem. Soc.* **2015**, *137*, 1572–1580.
- [19] N. L. Torad, R. R. Salunkhe, Y. Li, H. Hamoudi, M. Imura, Y. Sakka, C.-C. Hu, Y. Yamauchi, *Chem. Eur. J.* **2014**, *20*, 7895–7900.
- [20] M. Jin, H. Liu, H. Zhang, Z. Xie, J. Liu, Y. Xia, *Nano Res.* **2011**, *4*, 83–91.
- [21] M. E. Abdelsalam, S. Mahajan, P. N. Bartlett, J. J. Baumberg, A. E. Russel, *J. Am. Chem. Soc.* **2007**, *129*, 7399–7406.
- [22] D. Astruc, F. Lu, J. R. Aranzaes, *Angew. Chem. Int. Ed.* **2005**, *44*, 7852–7872; *Angew. Chem.* **2005**, *117*, 8062–8083.
- [23] K. K. R. Datta, M. Eswaramoorthy, C. N. R. Rao, *J. Mater. Chem.* **2007**, *17*, 613–615.
- [24] X. G. Hu, S. J. Dong, *J. Mater. Chem.* **2008**, *18*, 1279–1295.
- [25] X. M. Chen, G. H. Wu, J. M. Chen, X. Chen, Z. X. Xie, X. R. Wang, *J. Am. Chem. Soc.* **2011**, *133*, 3693–3695.
- [26] M. L. Toebes, J. A. van Dillen, Y. P. de Jong, *J. Mol. Catal. A* **2001**, *173*, 75–98.
- [27] M. J. Gronnow, R. Luque, D. J. Macquarrie, J. H. Clark, *Green Chem.* **2005**, *7*, 552–557.
- [28] Z. Chen, Z. M. Cui, F. Niu, L. Jiang, W. G. Song, *Chem. Commun.* **2010**, *46*, 6524–6526.
- [29] S. J. Guo, S. J. Dong, E. W. Wang, *ACS Nano* **2010**, *4*, 547–555.
- [30] B. P. Vinayan, R. Nagar, S. Ramaprabhu, *J. Mater. Chem. A* **2013**, *1*, 11192–11199.
- [31] C. Liu, Q. Ni, F. Bao, J. Qiu, *Green Chem.* **2011**, *13*, 1260–1266.
- [32] M. Maity, U. Maitra, *J. Mater. Chem. A* **2014**, *2*, 18952–18958.
- [33] M. Chitichigrovsky, Y. Lin, K. Ouchaou, M. Chaumontet, M. Robitzer, F. Quignard, F. Taran, *Chem. Mater.* **2012**, *24*, 1505–1510.
- [34] S. Das, S. Bhunia, T. Maity, S. Koner, *J. Mol. Catal. A* **2014**, *394*, 188–197.
- [35] S. J. Ye, D. Y. Kim, S. W. Kang, K. W. Choi, S. W. Han, O. O. Park, *Nanoscale* **2014**, *6*, 4182–4187.
- [36] M. S. Jin, H. Zhang, Z. X. Xie, Y. N. Xia, *Angew. Chem. Int. Ed.* **2011**, *50*, 7850–7858; *Angew. Chem.* **2011**, *123*, 7996–8000.
- [37] J.-J. Feng, D.-L. Zhou, H.-X. Xi, J.-R. Chen, A.-J. Wang, *Nanoscale* **2013**, *5*, 6754–6757.
- [38] Q. Wang, Y. Wang, P. Guo, Q. Li, R. Ding, B. Wang, H. Li, J. Liu, X. S. Zhao, *Langmuir* **2014**, *30*, 440–446.
- [39] S. Dutta, S. Sarkar, C. Ray, A. Roy, R. Sahoo, T. Pal, *ACS Appl. Mater. Interfaces* **2014**, *6*, 9134–9143.
- [40] R. D. Morgan, A. Salehi-Khojin, R. I. Masel, *J. Phys. Chem. C* **2011**, *115*, 19413–19418.
- [41] G. Hu, F. Nitze, H. R. Barzegar, T. Sharifi, A. Mikołajczuk, C.-W. Tai, A. Borodzinski, T. Wagberg, *J. Power Sources* **2012**, *209*, 236–242.
- [42] Q. Gao, M.-R. Gao, J.-W. Liu, M.-Y. Chen, C.-H. Cui, H.-H. Li, S.-H. Yu, *Nanoscale* **2013**, *5*, 3202–3207.
- [43] J. Chang, X. Sun, L. Feng, W. Xing, X. Qin, G. Shao, *J. Power Sources* **2013**, *239*, 94–102.
- [44] H. Qian, H. Huang, X. Wang, *J. Power Sources* **2015**, *275*, 734–741.
- [45] N. Karousis, G. E. Tsotsou, F. Evangelista, P. Rudolf, N. Ragoussis, N. Tagmatarchis, *J. Phys. Chem. C* **2008**, *112*, 13463–13469.
- [46] H. Jin, T. Xiong, Y. Li, X. Xu, M. Li, Y. Wang, *Chem. Commun.* **2014**, *50*, 12637–12640.
- [47] M. Liu, R. Zhang, W. Chen, *Chem. Rev.* **2014**, *114*, 5117–5160.
- [48] A. Chen, P. Holt-Hindle, *Chem. Rev.* **2010**, *110*, 3767–3804.
- [49] M. Gong, G. Fu, Y. Chen, Y. Tang, T. Lu, *ACS Appl. Mater. Interfaces* **2014**, *6*, 7301–7308.
- [50] A. Datta, S. Kapri, S. Bhattacharyya, *Green Chem.* **2015**, *17*, 1572–1580.
- [51] A. G. Sharpe, D. B. Wakefield, *J. Chem. Soc.* **1957**, 281–285.
- [52] T. Wang, Q. Zhou, X. Wang, J. Zheng, X. Li, *J. Mater. Chem. A* **2015**, *3*, 16435–16439.
- [53] C. Ray, S. Sarkar, S. Dutta, A. Roy, R. Sahoo, Y. Negishi, T. Pal, *RSC Adv.* **2015**, *5*, 12446–12453.
- [54] H. B. Pan, C. M. Wai, *New J. Chem.* **2011**, *35*, 1649–1660.
- [55] S. Fu, C. Zhu, D. Du, Y. Lin, *ACS Appl. Mater. Interfaces* **2015**, *7*, 13842–13848.
- [56] B. Xiong, Y. Zhou, Y. Zhao, J. Wang, X. Chen, R. O'Hayre, Z. Shao, *Carbon* **2013**, *52*, 181–192.
- [57] B. P. Vinayan, K. Sethupathi, S. Ramaprabhu, *Int. J. Hydrogen Energy* **2013**, *38*, 2240–2250.
- [58] Z. L. Li, J. H. Liu, Z. W. Huang, Y. Yang, C. Xia, F. W. Li, *ACS Catal.* **2013**, *3*, 839–845.
- [59] S. Dutta, C. Ray, A. Mondal, S. K. Mehetor, S. Sarkar, T. Pal, *Electrochim. Acta* **2015**, *159*, 52–60.
- [60] H. Huang, X. Wang, *J. Mater. Chem.* **2012**, *22*, 22533–22541.
- [61] Z. Liu, B. Zhao, C. Guo, Y. Sun, Y. Shi, H. Yang, Z. Li, *J. Colloid Interface Sci.* **2010**, *351*, 233–238.
- [62] C. Xu, L. Cheng, P. Shen, Y. Liu, *Electrochem. Commun.* **2007**, *9*, 997–1001.
- [63] Y. Lu, Y. Jiang, H. Wu, W. Chen, *J. Phys. Chem. C* **2013**, *117*, 2926–2938.
- [64] M. Zhao, K. Abe, S. Yamaura, Y. Yamamoto, *Chem. Mater.* **2014**, *26*, 1056–1061.
- [65] G. Z. Hu, F. Nitze, X. Jia, T. Sharifi, H. R. Barzegar, E. Gracia-Espino, T. Wagberg, *RSC Adv.* **2014**, *4*, 676–682.
- [66] Y. Liu, M. Chi, V. Mazumder, K. L. More, S. Soled, J. D. Henao, S. Sun, *Chem. Mater.* **2011**, *23*, 4199–4203.
- [67] E. Antolini, *Energy Environ. Sci.* **2009**, *2*, 915–931.

Manuscript received: February 11, 2016

Revised: March 5, 2016

Accepted Article published: March 27, 2016

Final Article published: April 23, 2016